University of BRISTOL

SCHOOL OF PHYSICS

FINAL YEAR PROJECT REPORT

NAME:	Darius Michienzi
DEGREE COURSE:	Physics with Astrophysics
PROJECT TITLE:	Exploring the new view of the X-ray universe
YEAR OF SUBMISSION:	2023
SUPERVISOR:	Ben Maughan
NUMBER OF WORDS:	4940



DECLARATION

As the sole member of this project all results and analysis which follows was preformed by myself alone. The raw data that was used is taken from public catalogues intended for academic use and is credited as such in the references to this report. The programs used to analyse the data are clearly noted and crediitited.

ACKNOWLEDGEMENTS

I wish to thank my supervisor Ben Maughan for his patience and guidance throughout the course of this project. I also wish to thank my sister Chelsey and good friend Zhe-Hui for help with proof reading and critiquing this report.

MNRAS **000**, 000–000 (0000) Preprint 27 October 2026 Compiled using MNRAS LATEX style file v3.0

Exploring the Effect of Optical Selection on X-ray Scaling Relations for Galaxy Clusters Using the eROSITA Telescope

D. M. Michienzi,[1]
H. H. Wills Physics Laboratory, University of Bristol, Tyndall Ave, Bristol BS8 1TL

19 April 2023

ABSTRACT

This project aims to compare the effect the selection method has on three different X-ray scaling relations. Those being the $L_X - kT$, $kT - \sigma_v$ and $L_X - \sigma_v$ relations. The GAMA catalogue is used to optically select the clusters, which are then spectrally analysed to find their X-ray Luminosity and ICM gas temperature. These are used to find the scaling relations which are compared to other findings when considering an X-ray selection. It is found that the selection method has little effect on the scaling relation value itself, although optical selection does appear to reduce the intrinsic scatter in the X-ray properties. Comparisons are also made to the self similar model for cluster evolution, which finds the $L_X - kT$ relation significantly different, while the other two cannot be ruled out as following this model.

1 INTRODUCTION

Galaxy clusters are the largest gravitationally bound objects in the universe. Their abundance and size are sensitive to cosmological parameters (such as the matter density Ω_M) and the conditions of the early universe as initial overdensities seed the position which, through successive mergers, clusters will form (See Kravtsov 2006; Vikhlinin et al. 2009; Planck Collaboration et al. 2016b, for more details). They also hold information about the formation and evolution of the galaxies within them from their internal dynamics as well as gas effects such as AGN feedback. The latter of the above discussed is easiest observed in the X-ray emission from the ionised gas which exists between the galaxies in a cluster known as the intra-cluster medium (ICM). It is for this reason galaxy clusters are often studied with X-ray telescopes such as eROSITA. the extended ROentgen Survey with an Imaging Telescope Array (eROSITA Predehl et al. 2021), part of the Spectrum-Roentgen-Gamma (SRG) mission, provides new opportunities to view large samples of galaxy cluster in X-ray wavelengths, as it is designed to view the whole sky in multiple passes, giving the most complete sample of X-ray sources to date.

The aim of this project is to use the eROSITA Final Equitorial-Depth Survey (eFEDS Liu et al. 2022) initial release data to demonstrate the ability for this new telescope to be used for cluster surveys and observations. It also aims to explore the selection method's impact on the scaling relations for X-ray properties of clusters from an optical and X-ray selection within the same eFEDS catalogue region.

Throughout this project the cosmology adopted is $H(z) = H_0 E(z) = H_0\sqrt{\Omega_M(1+z)^3 + \Omega_\Lambda}$. Where $H_0 = 70\text{kms}^{-1}\text{Mpc}^{-1}$, $\Omega_M = 0.3$ and $\Omega_\lambda = 0.7$. This is a close approximation of the standard flat ΛCDM found by Planck Collaboration et al. (2016a).

2 BACKGROUND

2.1 Scaling Relations

Scaling relations are a long standing technique to asses such large populations of clusters as a whole such as those expected to be generated by eROSITA. Scaling relations are simple power law proportionalities between two or more observable properties of clusters such as X-ray luminosity L_X and ICM temperature kT. These are useful in establishing relationships which can be then used to find properties which cannot be directly measured. For example measuring the flux distance to a cluster from a well calibrated $L_X - kT$ scaling relation for determining the expansion of the universe (Bora & Holanda 2023). Although they are described as empirical laws, it can be useful to use theoretical models to predict what we may expect Scaling relations to be. The most common model used is the self similar model, which states that all clusters are similar to each other, but have properties which scale proportionally to their mass (Lovisari & Maughan 2022). One key assumption of this model is that clusters form from single gravitational collapse and grow from hierarchical mergers with similar seized clusters (Kaiser 1986). This imposes self similarity with mass known as strong self similarity. Cluster scaling with the changing density of the universe through varying redshift is also a feature of the model known as weak self similarity (Bower 1997). Another assumption required for X-ray observations is that the only energy the ICM gains is from in-fall into the

© 0000 The Authors

cluster's gravitational potential. With these assumptions the following scaling relations with respect to mass similarity are predicted (see Lovisari & Maughan 2022, for a complete derivation).

$$kT \propto E^{\frac{2}{3}}(z)M^{\frac{2}{3}} \tag{1}$$

$$L_{X,soft} \propto E^2(z)M \tag{2}$$

$$L_{X,soft} \propto E(z)kT^{\frac{3}{2}} \tag{3}$$

Where $L_{X,soft}$ is the soft band X-ray luminosity (taken in this project to be the luminosity between 0.5-2.0 keV) hence referred to as just L_X. $E(z)$ is introduced into the relations to handle the weak self similarity of clusters by scaling the parameters according to the same factor the Hubble parameter changes with redshift. Directly measuring a cluster's total mass is often not possible, so instead for this project a proxy for the mass was used in the form of the cluster's velocity dispersion denoted σ_v. This is a measure of the standard deviation of the line of sight velocities of the galaxies within a cluster. This acts as a mass proxy as the higher the velocity dispersion, the more mass is required to gravitationally bind the cluster together and prevent the galaxies from flying apart. This proxy works based on the assumption clusters are relaxed, meaning they have had no recent mergers and the galaxies within them are somewhat spherically distributed. With this Equation 1 and Equation 2 will be modified as follows.

$$kT \propto \sigma_v^2 \tag{4}$$

$$L_X \propto E(z)\sigma_v^3 \tag{5}$$

The self similar model is not extensive in modelling all aspects of the dynamical evolution of clusters but it is still useful for comparing to observed scaling relations. This allows for testing which aspects of the model agree or disagree with observations and from this challenge or asses which assumptions are or are not correct.

2.2 Selection Method

The selection method describes how it is decided which clusters are chosen to be included in a sample. This must be considered carefully as this process may introduce bias to the sample. The most prescient to consider is Malmquist bias , which is the tendency for more intrinsically bright objects to be over represented in a sample as they are more likely to be observed (Malmquist 1922). If at lower temperatures, more intrinsically X-ray luminous clusters are over represented, this may lower the observed $L_X - kT$ scaling relation. A way which has been suggested to alleviate this is to change selection method to an optical selection method. This would involve finding clusters in optical wavelengths, then looking for an X-ray signature at the same position in the X-ray data. This should reduce bias as although the selection is still for optically bright or rich clusters, this is not directly correlated with the X-ray properties of a cluster.

While others (Andreon et al. 2016) have looked into selection effects on scaling relations these mostly look across samples taken from different catalogues in different regions of the sky. Little has been done to look into sampling bias when considering overlapping regions containing the same populations of clusters, selected for in different wavelengths. eROSITA provides for this opportunity as the whole sky survey in X-rays allows for any differently selected sample to have overlap with X-ray sampled data. This project therefore presents initial results in this area considering the smaller eFEDS catalogue (Liu et al. 2022) with hopes to expand in the future to look at the entire sky catalogue of eROSITA when it becomes available.

3 METHOD

3.1 Optical Selection

The specific selection method used was to select for clusters using the Galaxy And Mass Assembly (GAMA) catalogue (Driver et al. 2022). This is a catalogue of clusters seen in optical wavelengths, which was selected for having a section (G09) overlap and contained entirely with the eFEDS region. GAMA also directly measures the galaxy velocity dispersion σ_v for each cluster meaning this would not need to be separately measured. Taking the overlapping region, all clusters with a richness $\lambda \geq 20$ were selected for (measured in the number of friends-of-friends see Liske et al. 2015, for more details). Selecting the High richness clusters will mean selecting for more massive clusters with high flux, as galaxies will have to pass a specific optical flux limit to be able to be detected and included in richness counts. This limits the selection to clusters in the relatively nearby universe and will also eliminate smaller galaxy groups. This is done as these may have different intrinsic scaling relations (Lovisari et al. 2021) and also makes significant X-ray detection more likely, which is necessary due to the lower signal-to-noise ratio present in eROSITA data. This gave a total of 48 clusters from GAMA which were within the eFEDS region and therefore could be analysed.

3.2 Cluster Extent

With the position of clusters from GAMA marked in the eFEDS region, the luminosity L_X and gas temperature kT can be found from the X-ray emission. The approximate extent of each of the clusters is necessary to create a region from which X-ray data is extracted. For this the redshift and approximated mass M_{200} found by GAMA can be used to approximate R_{200} using Equation 6.

$$\frac{3M_\Delta}{4\pi R_\Delta^3} = \Delta\rho_c = \frac{3\Delta H^2(z)}{8\pi G} \tag{6}$$

With Δ in Equation 6 being 200. While this is a good starting point, the gas extent and therefore X-ray emissions generally extend only to R_{500} so by visual inspection as seen in Figure 1, $\frac{1}{2}R_{200}$ is taken to be the cluster's X-ray source extent. A background emission region is also required for each cluster. This is taken to be an annulus centred on the cluster with inner radius of $\frac{3}{4}R_{200}$ and outer radius $6R_{200}$ Point sources from within these region were identified from the eROSITA point source catalogue (Salvato et al. 2022) and excised so that the only emission considered from the

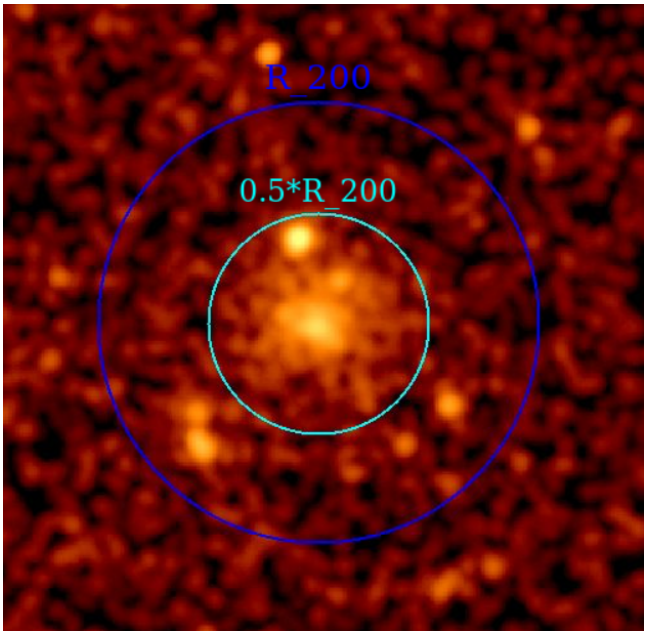


Figure 1. Image in $0.5-2.0$ keV X-ray range taken from eFEDS catalogue of the cluster GAMA 100001 showing how the extent of X-ray emission comes from $\frac{1}{2}R_{200}$.

source region is from the ICM, excluding any compact objects within the galaxies. This was also done for each background region.

3.3 Spectral Analysis

The spectra and response files were then extracted from the created source and background regions and used to fit to a spectral model to obtain the temperature and luminosity. `XSPEC` was used to fit an emission and absorption model. `PHABS` is used to model photoelectric absorption along the line of sight to the cluster from its redshift and the hydrogen column density from the `HEASOFT` *nh* function based of the HI4PI neutral hydrogen survey (HI4PI Collaboration et al. 2016). The `MEKAL` diffuse plasma model (Mewe et al. 1986; Liedahl et al. 1995) was used for the ICM emission taking a fixed metals abundance of 0.3 times solar abundances. This is used to find the temperature of the gas kT in keV. The `CLUMIN` convolution model was used to find the luminosity in the soft X-ray band L_X usually taken to be between $0.5-2.0$ keV. These values were fit to the spectral model between $0.2-4.0$ keV an example of which is shown in Figure 2.

Of the 48 initially selected clusters, 41 had significant enough X-ray emission to be successfully fit with this method, obtaining a luminosity and temperature to go along with its already known velocity dispersion. The 7 that could not were treated to a different method where at a reasonable fixed temperature, 2.0 keV, `CLUMIN` was again used to try and find an upper limit luminosity. With this, the upper limit was able to be found for 3 additional clusters giving overall 44 clusters with a luminosity value and 41 with a temperature value.

The full results are presented in Table B1 in section B of the appendix.

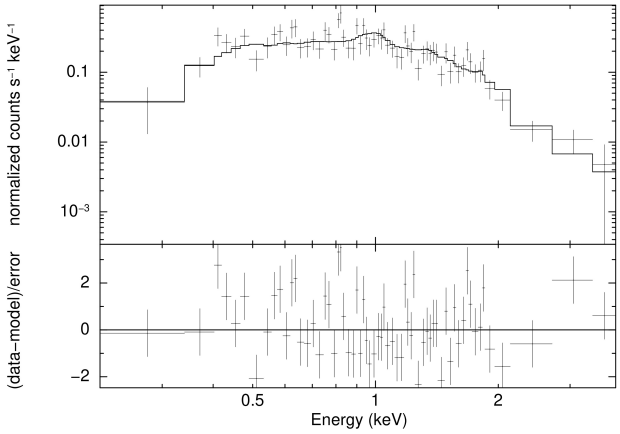


Figure 2. Energy spectra and residuals plot of cluster GAMA 100001 from 0.2-4.0 keV. The non constant binning is to ensure each bin contains at least 5 counts. From this particular spectra $L_X = 2.06 \pm 0.08$ erg/s and $kT = 2.65 \pm 0.39$ keV.

Y	X	γ	X_0	α	β	η
L_X	kT	1	1.84	43.02 ± 0.06	2.55 ± 0.37	0.11 ± 0.04
kT	σ_v	0	530	0.22 ± 0.03	1.45 ± 0.38	0.02 ± 0.01
L_X	σ_v	1	530	42.93 ± 0.07	2.94 ± 0.49	0.18 ± 0.05

Table 1. Table of the linear fitting parameters to Equation 7 for the 3 scaling relations seen in Figure 3

4 RESULTS

with obtained values for L_X, kT and σ_v the scaling relation power law can be found through plotting each in log-log space and finding the linear relationship between parameters. For this project a $\log_{10}$ space was used. In general each parameter relation was then fit to the linear equation 7.

$$log(\frac{Y}{E(z)^{\gamma}}) = \alpha + \beta log(\frac{X}{X_0}) \tag{7}$$

X_0 is the median value for each X parameter fit. This factor is considered in the linear fit to remove the degeneracy between the gradient β and the intercept α by placing the pivot for the linear fit in the centre of the data (see appendix section A for more details). The factor of $E(z)^{\gamma}$ accounts for the scaling with redshift with the power γ being the associated scaling parameter. For this paper weak self similarity was always assumed. Therefore the value of γ and X_0 is fixed for each relation and is shown in Table 1.

The `LINMIX` python module[2] was used co calculate the fit parameters using a hierarchical Bayesian approach (Kelly 2007). This provided the parameters to plot the linear fits seen in Figure 3.

The linear fit also provides the parameter η the intrinsic scatter. This is the remaining scatter seen in the points after the error has been accounted for. η is seen as the dashed

[2] See `https://linmix.readthedocs.io/en/latest/maths.html` for more details on the module specifically

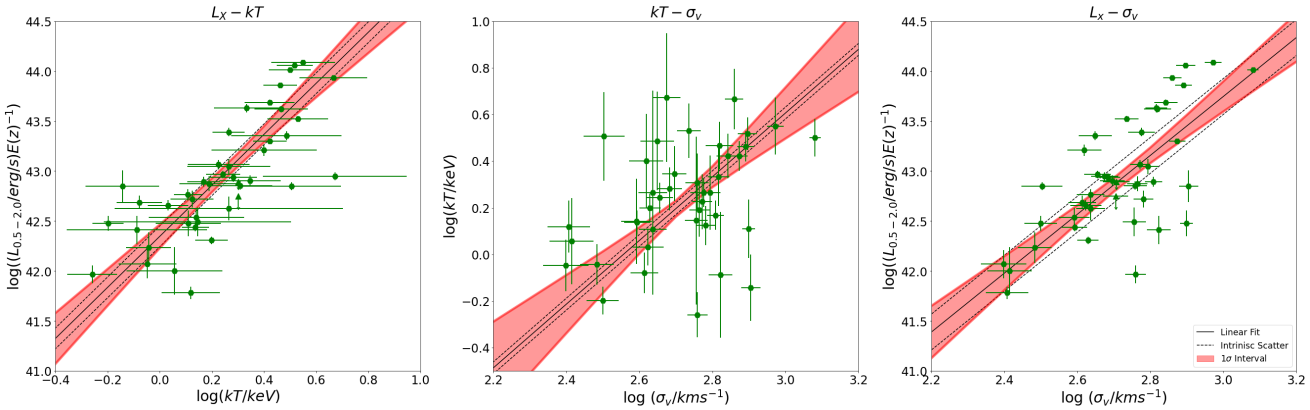


Figure 3. Plots for the three optically selected scaling relations described in Equation 3, Equation 5 and Equation 4. The solid black line represents the median value for the fitted gradient and intercept for the data which are presented in Table 1. The shaded red area is the 1σ confidence interval for these values while the the dotted black line represents the intrinsic scatter η.

lines in Figure 3. See section A in the appendix for more discussion of the degeneracy and error on these values.

5 DISCUSSION

5.1 Self Similar Comparison

It is useful to look initially into comparisons of the scaling relation to the self similar model. From Equation 3 the self similar model predicts a gradient of $\sim$ 1.5 for the $L_X - kT$ relation in log-log space. Equation 4 predicts the $kT - \sigma_v$ relation to be $\sim$ 2 while Equation 5 predicts the $L_X - \sigma_v$ relation to be $\sim$ 3. From the results in Table 1 it can be seen that the scaling relation for the $L_X - kT$ relation is significantly higher than what is predicted from the self similar model while the $kT - \sigma_v$ and $L_X - \sigma_v$ cannot be definitively said to be different from the predicted self similar relations when considering the 1σ intervals shown.

While the much larger gradient of the $L_X - kT$ relation is not consistent with the self similar model, it is consistent with many other observations of this relation (Lovisari et al. 2021; Eckmiller et al. 2011). This can be explained by challenging one of the assumption of the self similar model as discussed in subsection 2.1. The assumption being that the only energy input into the the ICM is from in-fall into the clusters gravitational well. Other energetic processes such as cluster mergers or AGN feedback (Planelles et al. 2014) are not accounted for in deriving this relation, so will not be reflected in the derived scaling relation . The effect of a process such as AGN feedback will be to increase both the temperature and X-ray luminosity of the ICM, but not necessarily in a way which will preserve the scaling relation. The net result seen is the steepening of the $L_X - kT$ relation as seen in Figure 3.

The inclusion of additional energy sources can explain the boost seen to $L_X - kT$ gradient, but raises questions about the apparent agreement of the other relations to the self similar model. If some other process is boosting the temperature and luminosity of the ICM beyond what is expected for self similarity, then this should reflect in the $kT - \sigma_v$ and $L_X - \sigma_v$ relations as a similar boost in the gradient from what is predicted as the effects describes should not influence σ_v in any way. To explain this consider the residuals plot shown in Figure 4. This shows a positive correlation (correlation coefficient of 0.70) between the residuals of the two scaling relations. This is saying that the clusters with an intrinsically high σ_v for their luminosity L_X also have a high σ_v for their temperature kT. This suggest there is also some underlying effect acting to boost the velocity dispersion σ_v independently from any self similarity for some of the clusters being considered. This would explain why these particular relations have greater agreement with the predicted self similar relation values while the $L_X - kT$ relation is so high. To explain this consider the assumption that all clusters considered are relaxed, which is necessary for σ_v to be used as an accurate proxy for the mass as discussed

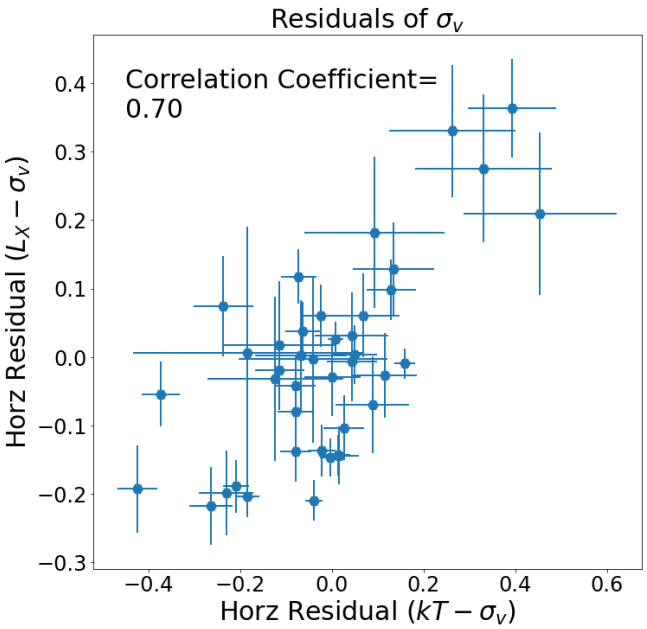


Figure 4. Plot of the horizontal residuals of the $L_X - \sigma_v$ plot in Figure 3 against the same residuals for the $kT - \sigma_v$ plot. The horizontal residual is the horizontal distance of the plotted point to the fit scaling relation shown as the black line in Figure 3.

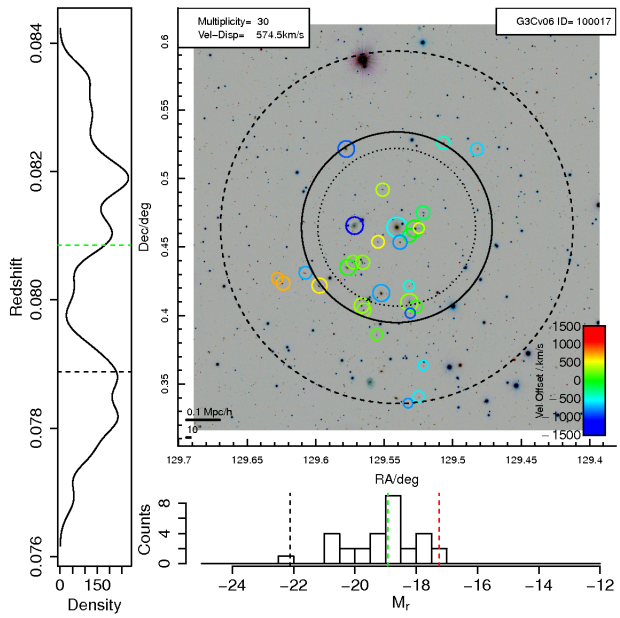


Figure 5. Entry from the GAMA catalogue of cluster GAMA 100017. The central image marks the position each member of the group is observed at coloured according to their relative line of sight velocity. The left hand bar shows the distributions of redshifts of the galaxies used to calculate the velocity dispersion σ_v

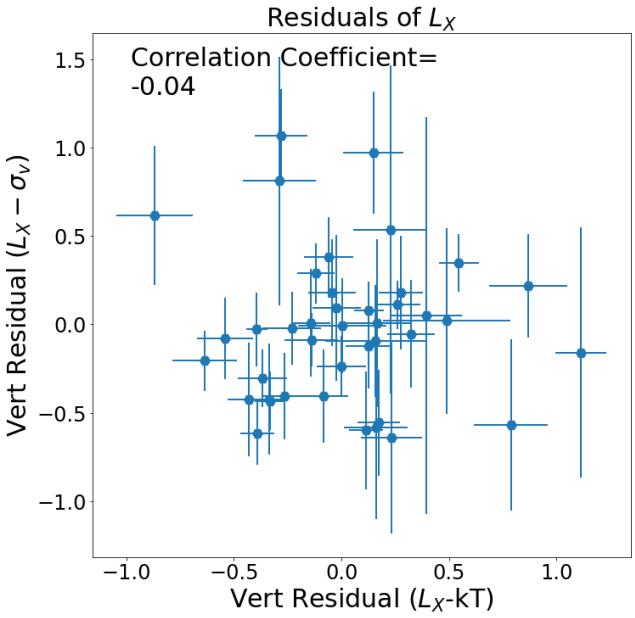


Figure 6. Plot of the vertical residuals of the $L_X - \sigma_v$ relation plotted against the vertical residuals of the $L_X - kT$ relation from Figure 3.

in subsection 2.1. If clusters are not relaxed, this would lead to internal galaxy velocities being not distributed normally and so larger velocity dispersion would be measured in comparison to the clusters actual mass. This can be seen to play at least a part in the correlation seen in Figure 4 by looking at the actual distribution of internal velocities of the most outlying point (furthest to the top right) from its GAMA catalogue entry in Figure 5. From this it can be seen that for this particular cluster the distribution of velocities are not well fit to a single normal distribution but in fact is probably best modelled by two normal distributions suggesting this is a cluster is possibly in the processes of merging with another. This is therefore the antithesis of a relaxed cluster so its velocity dispersion cannot be a good proxy for its mass, hence why it is at much higher σ_v for both its temperature and luminosity. This also being the case for other clusters provides an explanation for the underlying boost to σ_v. This result therefore suggests that most of the scatter in all of the relations is in the velocity dispersion.

Other residuals plots can be used to asses this scatter and the bias in the optically selected samples. Figure 6 shows the vertical residuals of the $L_X - \sigma_v$ relation plotted against the same residuals of the $L_X - kT$ relation in Figure 3. This shows no correlation between these two residuals. So clusters at a high L_X for their σ_v are not necessarily at a high L_X for their kT. This is interesting as σ_v and kT can be thought of as measurements of similar things as they both, in essence, measure the internal velocities of a cluster. One, however, is of the individual galaxies and is being measured from optical properties of the cluster while the other is of the gas in the cluster and is measured from its X-ray properties. This suggests that the scatter in X-ray and optical properties are independent of each other, pointing towards optical selection being a good method to reduce bias and scatter in measuring clusters' scaling relations.

5.2 $L_X - kT$ Relation

The Figure 7 shows a comparison of the scaling relation that was found through the optical selection of clusters from The GAMA catalogue and from a direct X-ray selection of the eFEDS region from Bahar et al. (2022). This is the most direct comparison possible between an optically and X-ray selected sample of galaxy clusters, given it is coming from the same region of sky and the same telescope. To compare the scaling relations directly the equation Bahar et al. found was re-scaled to the same median values to make direct comparisons. Using the same parameters as in Table 1 and the same fitting equation as in Equation 7 the X-ray selected data has $\alpha = 42.65 \pm 0.16$, $\beta = 2.93 \pm 0.12$ and $\eta = 0.80 \pm 0.07$. From comparisons to the results in Table 1 and visual inspection of Figure 7 the gradients are largely the same with the intercept of the optical selection being slightly higher. This suggests that while the optical selection has no effect on the scaling relation itself, the intercept is effected by the selection method. The optically selected data appears to be at the high end of luminoisties for the low end of temperatures. The optical selection method should be selecting for the more massive clusters and so it may be expected to be at the high end of temperatures if temperature is a good proxy for the mass of a cluster. Andreon et al. (2016) looked at a similar comparison of selection methods for a $L_X - M$ relation and found the opposite. The optically selected points were at the higher mass and luminosity end and showed a significantly different slope and there-

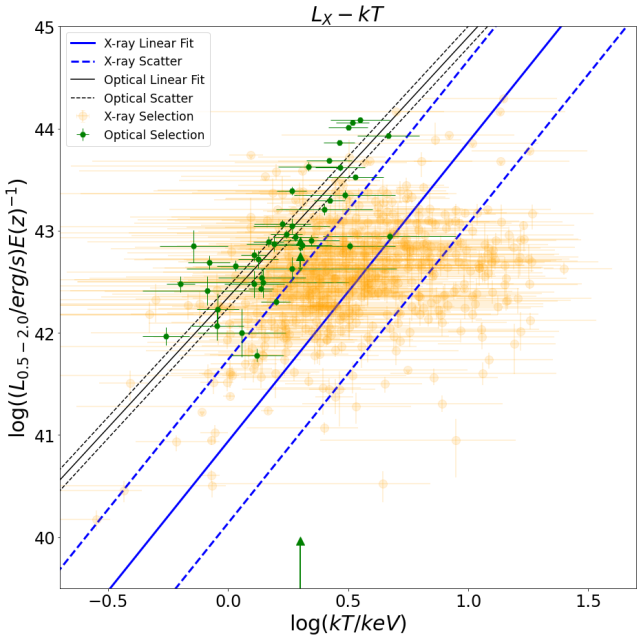


Figure 7. Comparison of the $L_X - kT$ scaling relation for the optical and X-ray selection of clusters from within the eFEDS region. The dotted lines in each case shows the intrinsic scatter The X-ray selected data is from Bahar et al. (2022).

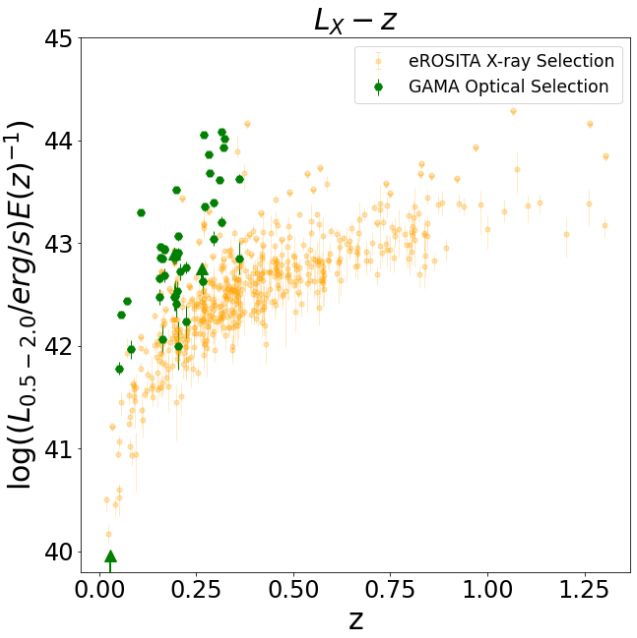


Figure 8. Plot of the X-ray luminosity against redshift for all the clusters in the X-ray and optically selected sample

fore power law relation. This comparison was for a selection of clusters from different regions and therefore populations, while the comparison here is of the same so this points to perhaps the change in slope Andreon et al. being an artefact their indirect comparison. However the position of the points at the low temperature end is still unusual if the predicted scaling relation holds, which it clear from Figure 3 it does. This may then be a product of the richness selection being set too high. To test this a comparison to X-ray selected data with a similar flux limit to that used bu GAMA should be used to then see whether a change in slope and intercept is seen.

Also note how the intrinsic scatter η for the optically selected sample is much lower than for the X-ray selected sample. This is the same result seen by Andreon et al.. This result is quite unexpected, as it would be expected the scatter in X-ray luminosity to be quite large for a selection from optical properties. This may or may not be a product of the optical selection itself, in this case, although the samples are of the same region and properties are taken from the same telescope, the span of the samples are very different. The X-ray selection covers a much larger number of clusters and covers a much larger range of redshifts and X-ray luminosities. This will mean the X-ray selection may include lower mass clusters, for which there is some evidence they may have different scaling relations which would increase the scatter seen. These smaller clusters may also have much larger errors on their measurement of values, such as temperature, due to them being fainter which would lead to the larger scatter which is seen.

Figure 8 shows a plot of the luminosity of a cluster against its redshift for the two samples considered here. This is use full to asses the Malmquist bias in a sample given that this is what is attempted to be reduced or eliminated by considering an optical selection. Looking at the X-ray selected data shows a clear flux limit and Malmquist bias as the lower luminosity clusters are only seen at the lowest redshifts, while there is a general non-linear trend upwards in luminosity as redshift increases. The optical selection does not show the exact same trend, but does appear to have a generally upward trend in luminosity for higher redshift. This may suggest the optical selection still suffers the same bias in luminosity, but the sample spans a much smaller redshift range and has a larger range of luminosities than the X-ray selection in that same band. Also, the optically selected clusters again appear to be on the more luminous end of the sample of X-ray clusters. This could be further evidence that the selection method discussed in subsection 2.2 is the cause of this observation. Ultimately, while it is clear the X-ray sample is bias in this way, it is difficult to tell whether the bias in the optical selection has been successfully in reducing this bias.

5.3 $kT - \sigma_v$ Relation

Direct comparison optically and X-ray selected clusters from the same eFEDS region using the eROSITA telescope is ideal in assessing the impact the selection method has on scaling relations. However, due to the recency of the eROSITA telescope, scaling relations involving σ_v from the eFEDS region and X-ray selcted could not be found to compare to. Instead data from different regions using the XXL survey (Pacaud et al. 2016) taken from the XMM-Newton telescope (Jansen et al. 2001) were found and used in the preceding sections.

Figure 9 shows a comparison of the optically selected fit scaling relations for the $kT - \sigma_v$ relation to that of an X-ray selected sample of clusters from the XXL survey (Wilson et al. 2016). The fit line, again re-scaled to have a direct

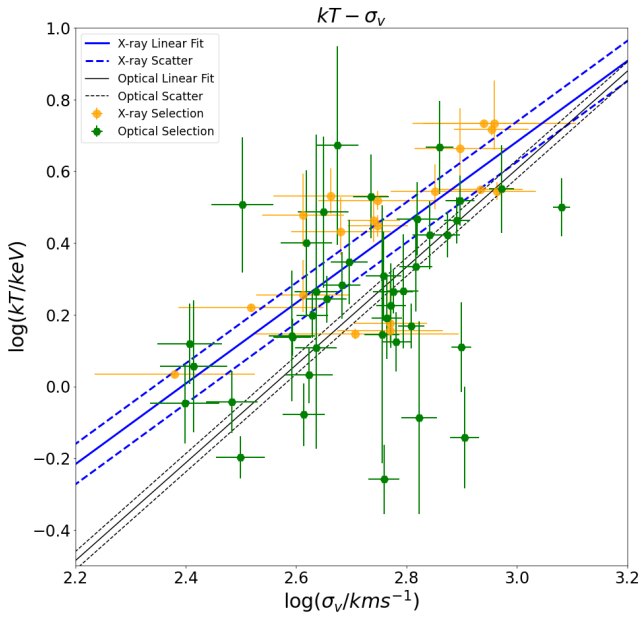


Figure 9. Comparison of the $kT - \sigma_v$ scaling relation for the optical and X-ray selection of clusters. The X-ray selected data is from a different region of sky to the optical in the XXL Survey Wilson et al. (2016).

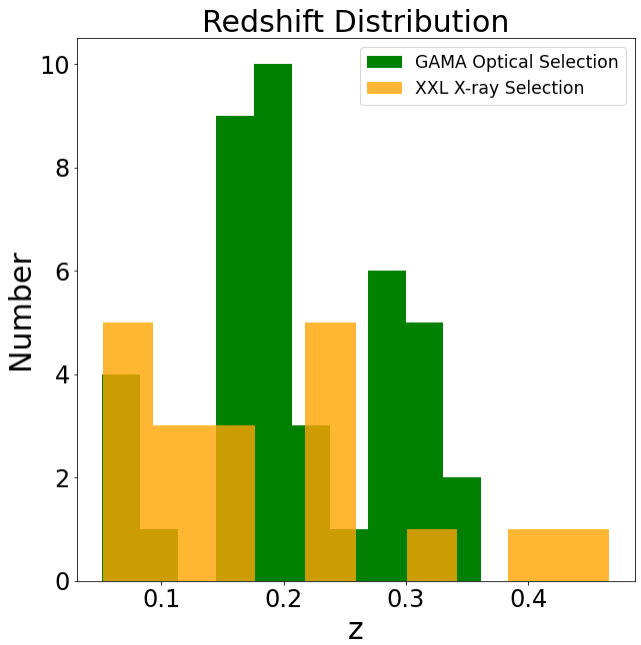


Figure 10. Histogram showing the distribution of redshifts for clusters selected for in X-rays and optical. The optical selection is from the GAMA catalogue overlapping the eFEDS region while the X-ray selection is from the XXL survey as discussed in Wilson et al. (2016).

comparison, gives $\alpha = 0.37 \pm 1.15$, $\beta = 1.12 \pm 0.20$ and $\eta = 0.05 \pm 0.03$. The gradients again cannot be said to be definitively different from each other suggesting the optical selection has made no difference to these values. There is also no clear difference in the intercept values. The X-ray selected cluster is slightly higher than the optical selection and has a much larger measurement error due to the fitting which was preformed being for the reverse relation $\sigma_v - kT$ rather than $kT - \sigma_v$. Direct comparison of these intercept values is not possible as different telescopes often give different temperature values when observing the same object due to calibration discrepancies. Turner et al. (2022) finds that clusters in measured by XMM-Newton may be measured as being 25±9% hotter than those measured by eROSITA. This may account entirely for the slightly elevated intercept for the X-ray selected data or indicate that in fact the optical selection is leading to a boosted intercept as in subsection 5.2. This demonstrates why direct comparison is more desirable as without it, the exact scenario is impossible to know.

The intrinsic scatter is again lower for the optically selected data than the X-ray selected data. This is a more true indication of optical selection reducing scatter, as the samples here are much more similar in size and Figure 10 shows how the clusters considered also span a similar range of redshifts. From visual inspection the errors on each value appear roughly similar, so the reason for this lower scatter remains again unknown. The one caveat again is the lack of direct comparison as the eFEDS region and XXL do not overlap, so different populations of clusters are being considered.

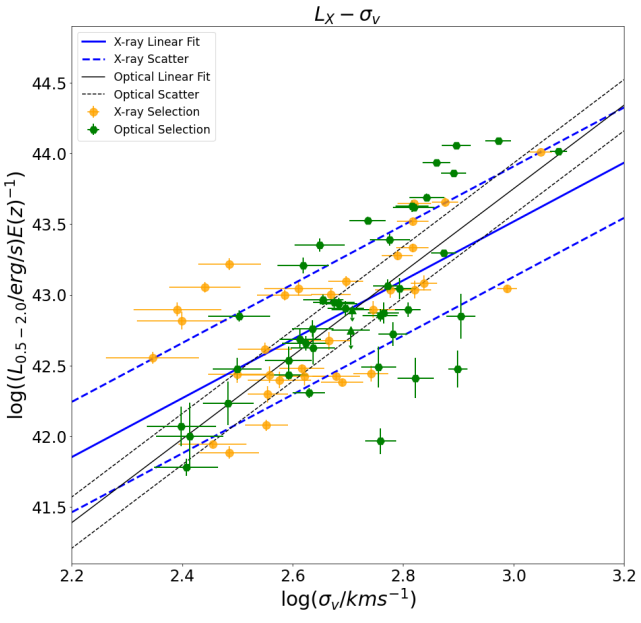


Figure 11. Plot the comparison of the $L_X - \sigma_v$ scaling relation for the optical and X-ray selection of clusters. The X-ray selected data is from a different region of sky to the optical in the XXL Survey Giles et al. (2022)

5.4 $L_X - \sigma_v$ Relation

The optical selection for the $L_X - \sigma_v$ is compared to the same relation of X-ray selection of clusters in XXL from Giles et al. (2022). They found the values $\alpha = 42.94 \pm 0.30$, $\beta = 2.08 \pm 0.48$ and $\eta = 0.89 \pm 0.06$. The normalisation value α are almost exactly the same for these two values. The gradients are also not significantly different from one another. The scatter η is again significantly lower for the optically selected clusters, suggesting also that the optical selection somehow reduces this intrinsic scatter. This can be contrasted additionally with Andreon et al. (2016) who finds different gradients between the two selections and data on the larger end of mass, in this case σ_v. Here the comparison also is to two different regions and so is not a direct comparison, but yet again the results dispute the findings of Andreon et al..

It is interesting to note that for the $L_X - \sigma_v$ and the $kT - \sigma_v$ relation discussed in subsection 5.3 there is in general agreement between the X-ray and optical selection of the clusters for both when using σ_v as a mass proxy. This suggests that the morphological differences, which is suggested to lead to deviations from the self similar model, must be the same across the two selection methods. This may mean a fixed and unbiased proportion of clusters are unrelaxed, which has implications for how these clusters merge and evolve with time, which could be explored in future studies.

To asses the effectiveness of optical selection in reducing Malmquist bias in this sample a plot similar to Figure 8 plotting the luminosity against redshift can be made. Figure 12 shows such a plot. From the plot, it is difficult to conclude whether the X-ray selected sample is in this way biased or whether the optical selection is in anyway different, as both appear to span a similar redshift and luminosity range. It is possible to say that both samples are similar to each other as both sets of points sit together.

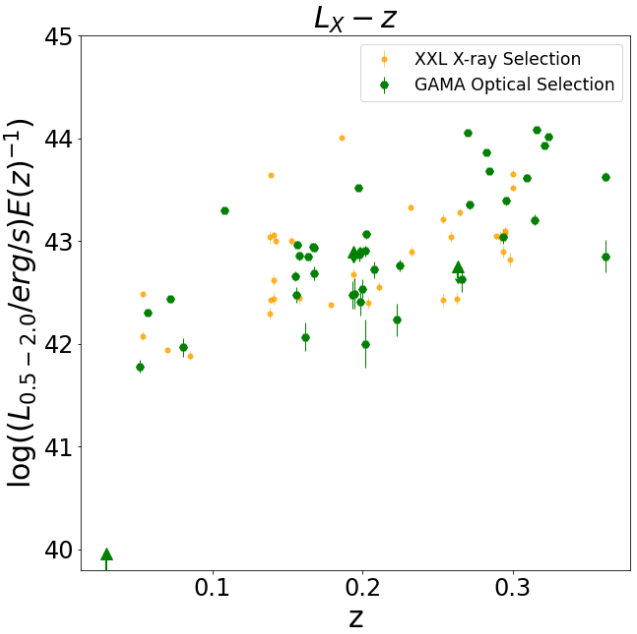


Figure 12. Plot of the X-ray luminosity against redshift for all the clusters in the X-ray and optically selected sample

6 CONCLUSION

6.1 Self Similarity

Comparisons of the found scaling relations to the self similar model reinforce previous findings of the $L_X - kT$ relation in reality being significantly higher as seen in Table 2. The explanation of additional energy sources not considered by the model does seem reasonably fit, looking into what proportion of the clusters viewed actually contain AGN would be necessary to confirm this hypothesis. The other scaling relations cannot be said to be significantly different to what is predicted.

The Scatter in the velocity dispersion can be largely attributed to the inclusion of unrelaxed clusters in the sample, which acts to give them high a σ_v for their mass. Since the self similar model is predicated on self similarity with mass scale, the scaling relations involving σ_v cannot be said to be direct comparisons to the self similar model. In future, obtaining direct measurements of a clusters mass would be more desirable for comparisons to the self similar model.

6.2 Selection Method

While the aim of this project was to compare selection method's effects on scaling relations from an optical and X-ray selection, this could only be accurately done for the $L_X - kT$ relation, as this was the only relation for which the same catalogue (eFEDS) was used for both the X-ray and optical selection. This relation power law, seen in Table 2, shows no significant difference between the two selection methods. The X-ray selection's power law is larger, but not by a significant amount when considering the errors taken into account. It is a similar case for the other relations, although they are not direct comparisons as discussed. Some such as Andreon et al. (2016) have suggested that optical selection should lead to larger power scaling relations. This is not supported by the findings of this project with in fact the $L_X - kT$ relation having a larger gradient in the X-ray selected sample.

What is supported is that optically selected samples have lower intrinsic scatter as seen in Table 2. This could be explained if the optically selected data had much larger error associated with the fit values, as this would mean that the scatter in values could be largely accounted for in the error. This, however, is not seen suggesting that optical selection is more likely to pick clusters which form low scatter scaling relations. A way to test this in future study would be to simply take larger samples of both X-ray and optically selected clusters to reduce random error as much as possible.

6.3 Further Study

The conclusions which can be made are limited by the fact that direct comparison of similar populations of clusters from the two selection methods discussed was not possible. eROSITA ultimately will be very useful in providing

Relation	α_{opt}	α_X	β_{opt}	β_X	β_{Self}	η_{opt}	η_X
$L_X - kT$	43.02 ± 0.06	42.65 ± 0.16	2.55 ± 0.37	2.93 ± 0.12	1.5	0.11 ± 0.04	0.80 ± 0.07
$kT - \sigma_v$	0.22 ± 0.03	0.37 ± 1.15	1.45 ± 0.38	1.12 ± 0.20	2.0	0.02 ± 0.01	0.05 ± 0.03
$L_X - \sigma_v$	42.94 ± 0.07	42.94 ± 0.30	2.94 ± 0.49	2.08 ± 0.48	3.0	0.18 ± 0.05	0.89 ± 0.06

Table 2. Overall comparison for the fit values for the three scaling relations considered. The subscript *opt* for those pertaining to the optical selection and X is for the X-ray selection. β_{Self} is the predicted self similar scaling relation power law

for this opportunity when the full sky survey is released. By providing a large catalogue of clusters, which covers the whole sky, from which X-ray properties can be derived, any other optical catalogue can be used as for optical selection to compare the method to. Choosing an optical catalogue with mass measurements will also mean comparisons of all the self similar scaling relations between the two selection method will be able to be made. Further study of this will therefore be able to draw much more conclusive results about how selection effects scaling relations, scatter and bias.

REFERENCES

Andreon S., Serra A. L., Moretti A., Trinchieri G., 2016, A&A, 585, A147
Bahar Y. E., et al., 2022, A&A, 661, A7
Bora K., Holanda R. F. L., 2023, European Physical Journal C, 83, 274
Bower R. G., 1997, MNRAS, 288, 355
Driver S. P., et al., 2022, MNRAS, 513, 439
Eckmiller H. J., Hudson D. S., Reiprich T. H., 2011, A&A, 535, A105
Foreman-Mackey D., 2016, The Journal of Open Source Software, 1, 24
Giles P. A., et al., 2022, MNRAS, 511, 1227
HI4PI Collaboration et al., 2016, A&A, 594, A116
Jansen F., et al., 2001, A&A, 365, L1
Kaiser N., 1986, MNRAS, 222, 323
Kelly B. C., 2007, ApJ, 665, 1489
Kravtsov A. V., 2006, arXiv e-prints, pp astro–ph/0607463
Liedahl D. A., Osterheld A. L., Goldstein W. H., 1995, ApJ, 438, L115
Liske J., et al., 2015, MNRAS, 452, 2087
Liu A., et al., 2022, A&A, 661, A2
Lovisari L., Maughan B. J., 2022, in , Handbook of X-ray and Gamma-ray Astrophysics. Edited by Cosimo Bambi and Andrea Santangelo. p. 65, doi:10.1007/978-981-16-4544-0˙118-1
Lovisari L., Ettori S., Gaspari M., Giles P. A., 2021, Universe, 7, 139
Malmquist K. G., 1922, Meddelanden fran Lunds Astronomiska Observatorium Serie I, 100, 1
Mewe R., Lemen J. R., van den Oord G. H. J., 1986, A&AS, 65, 511
Pacaud F., et al., 2016, A&A, 592, A2
Planck Collaboration et al., 2016a, A&A, 594, A13
Planck Collaboration et al., 2016b, A&A, 594, A24
Planelles S., Borgani S., Fabjan D., Killedar M., Murante G., Granato G. L., Ragone-Figueroa C., Dolag K., 2014, MNRAS, 438, 195
Predehl P., et al., 2021, A&A, 647, A1
Salvato M., et al., 2022, A&A, 661, A3
Turner D. J., et al., 2022, MNRAS, 517, 657
Vikhlinin A., et al., 2009, ApJ, 692, 1060
Wilson S., et al., 2016, MNRAS, 463, 413

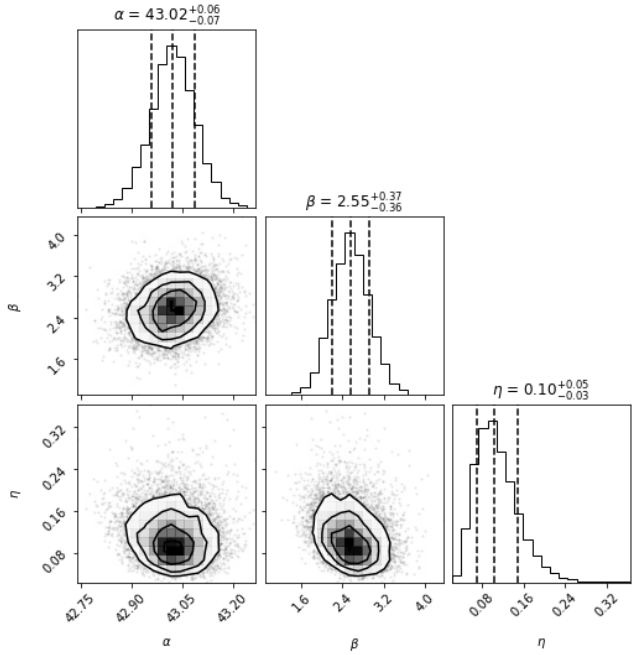


Figure A1. Corner plot for the parameters fit in Equation 7 for the $L_X - kT$ scaling relation. The dotted lines show the 84.1 and 15.9 percentiles

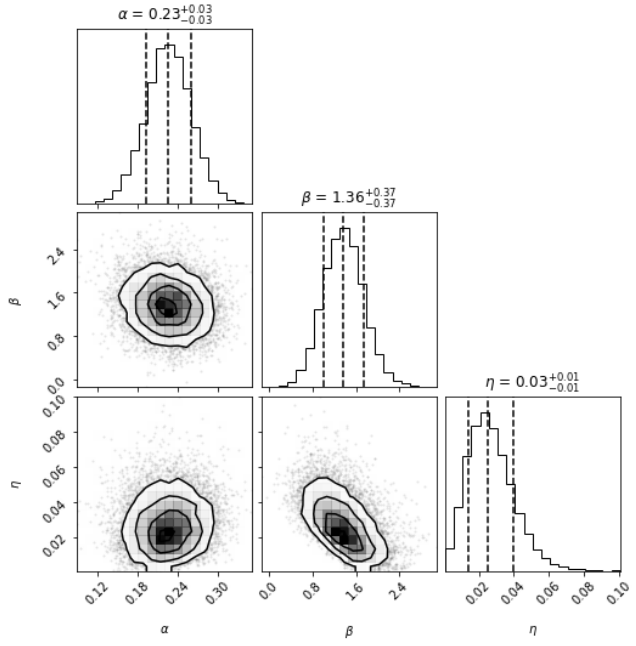


Figure A2. Corner plot for the parameters fit in Equation 7 for the $kT - \sigma_v$ scaling relation. The dotted lines show the 84.1 and 15.9 percentiles

APPENDIX A: CORNER PLOTS

The corner plots are shown in Figures A1, A2 and A3 were created using the `corner.py` library created by Foreman-Mackey (2016). These plots show how by dividing by the median value X_0 (as shown in Equation 7) for each scaling relation, the degeneracy between the intercept α and slope β can be removed evident in the fact the scatter plots between these two parameters are circularly symmetric. From the histograms it can be seen the deviation in these values are well modelled by a normal distribution hence why the 84.1 and 15.9 percentiles are roughly the same distance from the mean and so can be taken as the usual 1σ intervals. The minimum value η can take is 0, and for all the relations the value of η is small hence why it is a slightly uneven distribution. The differences in the two percentiles given for η are also close enough that the average of these is taken as the 1σ intervals for these values. There is some evidence of degeneracy between the values of β and η for the $kT - \sigma_v$ relation but since these values are never compared to each other this can be ignored.

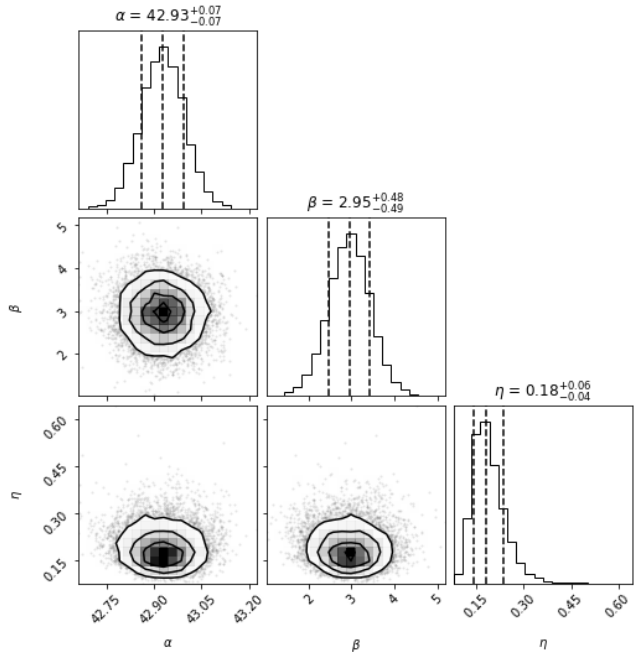


Figure A3. Corner plot for the parameters fit in Equation 7 for the $L_X - \sigma_v$ scaling relation. The dotted lines show the 84.1 and 15.9 percentiles

APPENDIX B: TABLE OF RESULTS

Table showing the position and obtained values of L_X, kT and σ_v for each of the clusters in this paper. They are arranged in descending order of richness as this is how they were selected from the GAMA cataloge.

Table B1. Table showing the ID, position (RA and DEC), richness, redshift (z) and velocity dispersion (σ_v) for all clusters selected from GAMA with richness $\lambda \geq 20$. It also shows the output values of X-ray luminosity in the 0.5-2.0 keV band (L_X), and the ICM temperature (kT) from the spectral analysis. The values of 2.0 in kT column indicate clusters for which the initial spectral fitting failed and so a fixed temperature was chosen to obtain an upper limit on the luminosity.

GAMA ID	RA	DEC	Richness	z	σ_v kms^{-1}	$Log(\frac{L_X}{erg/s})$	kT keV
100003	138.520	-0.024	76	0.168	410 ± 36	42.72 ± 0.07	0.83 ± 0.17
100001	133.653	0.643	62	0.108	750 ± 39	43.32 ± 0.02	2.65 ± 0.39
100002	132.600	0.260	59	0.197	540 ± 41	43.57 ± 0.03	3.38 ± 0.91
100009	129.889	-1.679	55	0.270	780 ± 48	44.12 ± 0.02	3.29 ± 0.53
100006	134.521	1.154	54	0.072	390 ± 31	42.45 ± 0.04	1.37 ± 0.16
100011	140.545	-0.460	53	0.321	720 ± 42	44.00 ± 0.02	4.64 ± 1.39
100044	140.652	-0.409	46	0.057	430 ± 29	42.32 ± 0.04	1.58 ± 0.23
100019	139.073	-0.402	41	0.324	1210 ± 43	44.09 ± 0.02	3.16 ± 0.59
100018	138.379	2.753	39	0.156	320 ± 32	42.51 ± 0.08	0.63 ± 0.09
100004	131.435	-0.488	37	0.156	450 ± 38	43.00 ± 0.04	1.75 ± 0.26
100075	132.628	0.638	35	0.194	570 ± 42	42.53 ± 0.14	1.40 ± 1.16
100027	134.035	0.430	35	0.168	480 ± 38	42.97 ± 0.04	1.91 ± 0.41
100013	140.207	2.754	34	0.283	780 ± 41	43.92 ± 0.02	2.90 ± 0.43
100010	136.929	1.558	34	0.164	320 ± 41	42.88 ± 0.04	3.21 ± 1.4
100005	135.503	2.393	34	0.203	590 ± 37	43.11 ± 0.05	1.68 ± 0.46
100007	135.378	-1.655	33	0.316	940 ± 50	44.16 ± 0.02	3.55 ± 1.0
100032	138.610	2.922	32	0.162	250 ± 36	42.10 ± 0.14	0.90 ± 0.23
100008	133.364	-0.356	31	0.194	510 ± 42	42.94 ± 0.06	2.0
100037	133.431	2.399	30	0.198	580 ± 37	42.92 ± 0.07	1.55 ± 0.41
100025	131.692	1.831	30	0.052	260 ± 34	41.79 ± 0.06	1.32 ± 0.34
100024	136.503	0.016	30	0.202	500 ± 38	42.95 ± 0.05	2.22 ± 0.6
100017	129.541	0.464	30	0.081	570 ± 37	41.98 ± 0.09	0.55 ± 0.12
100141	134.412	2.150	27	0.202	260 ± 36	42.04 ± 0.24	1.14 ± 0.48
100012	140.152	-1.251	27	0.155	420 ± 41	42.69 ± 0.05	1.08 ± 0.19
100021	139.761	2.820	26	0.200	390 ± 38	42.58 ± 0.09	1.38 ± 0.58
100016	137.307	-0.206	26	0.309	660 ± 57	43.69 ± 0.03	2.93 ± 0.69
100015	139.709	2.201	26	0.284	700 ± 51	43.75 ± 0.03	2.64 ± 0.58
100014	133.126	0.420	26	0.272	450 ± 47	43.41 ± 0.05	3.06 ± 1.49
100036	140.682	2.132	24	0.199	640 ± 35	42.94 ± 0.05	1.47 ± 0.21
100035	133.850	1.831	23	0.264	500 ± 41	42.81 ± 0.11	2.0
100030	129.923	1.074	23	0.158	570 ± 42	42.89 ± 0.04	2.03 ± 0.58
100026	130.427	0.477	23	0.208	600 ± 37	42.77 ± 0.08	1.33 ± 0.25
100212	129.905	2.813	22	0.193	790 ± 32	42.52 ± 0.13	1.29 ± 0.37
100040	139.344	1.024	22	0.362	660 ± 45	43.71 ± 0.04	2.16 ± 0.62
100023	138.467	-0.760	22	0.296	600 ± 50	43.46 ± 0.04	1.84 ± 0.26
100116	131.683	2.537	21	0.029	210 ± 24	40 ± 20	2.0
100063	134.696	0.057	21	0.266	430 ± 40	42.68 ± 0.12	1.84 ± 1.86
100038	137.773	0.251	21	0.223	300 ± 33	42.28 ± 0.15	0.91 ± 0.18
100020	138.514	1.645	21	0.167	470 ± 41	42.98 ± 0.04	4.7 ± 2.99
100066	131.204	1.001	20	0.293	620 ± 40	43.11 ± 0.08	1.84 ± 0.67
100043	129.342	1.594	20	0.362	800 ± 48	42.93 ± 0.16	0.72 ± 0.23
100033	140.398	-0.242	20	0.315	410 ± 45	43.28 ± 0.06	2.51 ± 1.17
100028	134.622	-1.118	20	0.225	430 ± 38	42.81 ± 0.06	1.28 ± 0.16
100022	139.430	0.796	20	0.199	660 ± 50	42.46 ± 0.14	0.82 ± 0.51

CERTIFICATION OF OWNERSHIP OF THE COPYRIGHT

This Project Report is presented as part of, and in accordance with, the requirements for the degree of MSci at the University of Bristol, Faculty of Science.

I hereby assert that I own exclusive copyright in the item named below. I give permission to the University of Bristol Library to add this item to its stock and to make it available for consultation in the library, and for inter-library lending for use in another library. I also give consent for this report to made available electronically to staff and students within the University of Bristol. It may be copied in full or in part for any bona fide library or research work. No quotation and no information derived from it may be published without the author's prior consent.

Author	Darius Michienzi
Title	Exploring the new view of the X-ray universe
Date of submission	19/04/2023
Signature	D.Michienzi

I agree that submission of this report constitutes signing of this declaration.

This project is the property of the University of Bristol and may only be used with due regard to the rights of the author. Bibliographical references may be noted, but no part may be copied for use or quotation in any published work without the prior permission of the author. In addition, due acknowledgement for any use must be made.